Mg/Air Battery Materials

DOI: 10.1002/ange.200600099

Metallic Magnesium Nano/Mesoscale Structures: Their Shape-Controlled Preparation and Mg/Air Battery Applications**

*Weiyang Li, Chunsheng Li, Chunyuan Zhou, Hua Ma, and Jun Chen**

Metal nano/mesoscale structures have received intense attention because of the novel physical and chemical properties that are not present in their corresponding macroscale structures.[1–4] Magnesium is one of the most intriguing alkaline-earth metals and has found applications in the fields of H_2 storage, organic synthesis, biochemistry, and as an electrode material.[5–8] With respect to Mg nanomaterials, most studies have focused on the fabrication of Mg nanoparticles[9] and related nanocomposites by high-energy milling methods.[10] It should also be noted that theoretical research on Mg nanowires has been done by computer simulation.[11] However, to the best of our knowledge, there are no reports in the literature on the preparation of Mg nano/mesostructures with controlled shape and morphology.

The field of electrochemical storage and generation of energy in batteries is gaining tremendous importance for powering high-tech electronic devices and for enabling a greener transportation industry.[12] Among various batteries, the Mg/air battery system has the advantages of a high theoretical voltage (3.09 V) and energy density (3910 $Wh\,kg^{-1}$), low cost, light weight, and environmental friendliness.[13] It is a special feature of the Mg/air battery that only the active component of the negative electrode (Mg) needs to be stored in the battery, while the reactant (O_2) for the positive (bifunctional oxygen-diffusion) electrode during discharge is drawn from the air by a reduction reaction.[14] It is therefore of great scientific and technological importance to improve the properties of the Mg electrode so as to enhance the performance of Mg/air batteries. Herein, we describe the first example of the shape-controlled preparation of Mg nano/mesoscale structures and their promising properties for application in Mg/air batteries.

The various Mg structures were prepared by a simple vapor-transport approach using commercially available Mg powder and no templates or catalysts (see Supporting Information). The size and morphology of the products are predominantly controlled by the experimental conditions (see Supporting Information). The evaporation temperature was fixed at 850 and 950 °C, and the products were deposited in the cooler region of the stainless-steel tube at a temperature of around 300 °C.

Figures 1a and b show typical SEM images of the as-synthesized Mg spheres (sample A) and plates (sample B) prepared at an evaporation temperature of 850 °C with different flow rates of Ar gas (sample A: 400 $cm^3\,min^{-1}$; sample B: 800 $cm^3\,min^{-1}$). It can be seen that both the spheres and the plates are distributed homogeneously over a wide area. The spheres are polyhedra with a diameter of approximately 200–500 nm and the plates have a smooth surface and a regular hexagonal shape with a diameter in the range of 150–460 nm. When the evaporation temperature was increased to 950 °C, Mg nanorods (sample C) and sea-urchin-like nanostructures (sample D) were obtained at Ar flow rates of 400 and 800 $cm^3\,min^{-1}$, respectively. Figure 1c displays a representative SEM image of the as-prepared Mg nanorods, which reveals that the sample contains short,

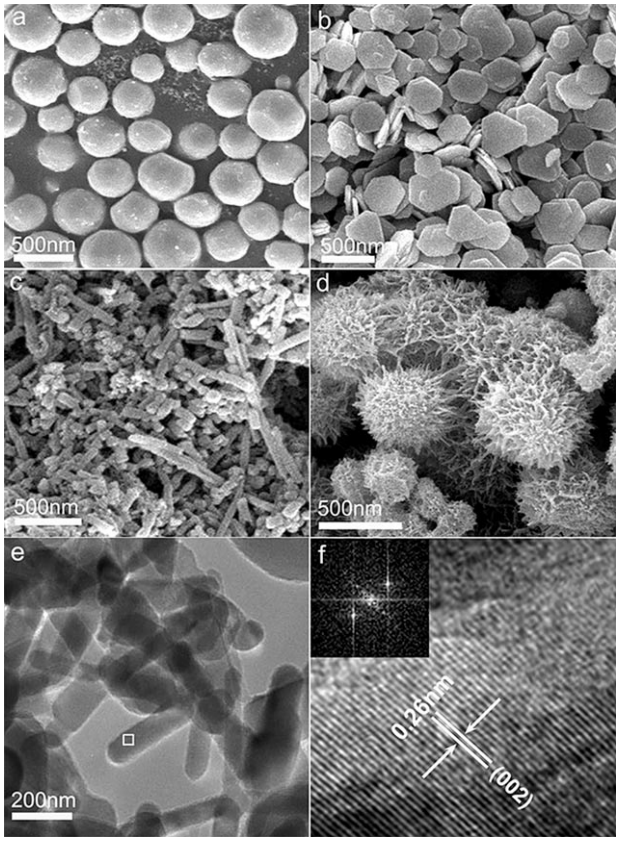

Figure 1. Typical scanning electron microscopy (SEM) images of the as-prepared Mg products: sample A (a), sample B (b), sample C (c), sample D (d); representative transmission electron microscopy (TEM) image of sample C (e) and high-resolution transmission electron microscopy (HRTEM) image (f) of the white square marked in (e); the inset in (f) shows the corresponding fast Fourier transform (FFT) pattern.

[*] W. Li, C. Li, C. Zhou, Dr. H. Ma, Prof. Dr. J. Chen
Institute of New Energy Materials Chemistry
Nankai University
Tianjin 300071 (P.R. China)
Fax: (+86) 22-2350-9118
E-mail: chenabc@nankai.edu.cn

[**] This work was supported by the NSFC (20325102 and 90406001) and the 973 Program (2005CB623607). W.L. and C.L. contributed equally to this work. We are also very grateful to the reviewers for their valuable suggestions.

Supporting Information for this article is available on the WWW under http://www.angewandte.org or from the author.

uniform, rodlike structures with a length of approximately 200–500 nm. The SEM image of the Mg sea-urchin-like nanostructures (Figure 1 d) shows their prickly, spherical morphology with very fine whiskerlike fibrils of several tens of nanometers in length. Moreover, these nanowhiskers are interconnected to form a porous network architecture. The TEM image of sample C (Figure 1 e) shows that the diameter of the nanorods is in the range 70–100 nm. The HRTEM image in Figure 1 f shows clear fringes with an interplanar spacing of 0.26 nm, which corresponds to the separation between the (002) lattice planes. These are aligned perpendicular to the longitudinal direction of the rod, which suggests that the nanorods grow along the [001] direction.

When maintaining the experimental conditions for preparing the above four different Mg structures but extending the heating time to 2 h, various other Mg micro/nanostructures with different sizes and morphologies were obtained (see Supporting Information). The prevailing growth morphology of the as-prepared Mg micro/nanostructures is strongly influenced by the degree of supersaturation in the vapor-transport approach, and this is mainly controlled by the experimental parameters, including both the evaporation and deposition temperature, the flow rate of the carrier gas, and the heating time.[15]

Figure 2 shows representative XRD patterns of the as-prepared Mg structures. It can be seen that the positions of the characteristic peaks of the four products are identical. All

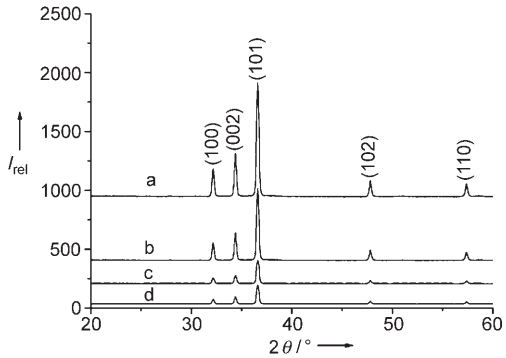

Figure 2. X-ray diffraction (XRD) patterns of the as-prepared Mg products: sample A (a), sample B (b), sample C (c), and sample D (d).

the diffraction peaks can be readily indexed on the basis of the hexagonal close-packed structure of Mg (ICDD-JCPDS 35-0821). No peaks from other phases can be detected, thus indicating that the products are of high purity. According to the present observations, a lower evaporation temperature leads to the formation of products with a larger grain size (samples A and B), while a higher evaporation temperature leads to a smaller grain size (samples C and D). BET nitrogen-adsorption measurements show that the specific surface areas of samples A–D are 8.4, 15.6, 47.2, and 130.6 $m^2 g^{-1}$, respectively.

With respect to metal/air batteries, considerable research effort has been devoted to the study of the performance of Zn/air and Al/air batteries.[16] However, only a few studies have focused on Mg/air batteries.[17] The electrochemical reactions of the Mg/air battery can be expressed by Equations (1)–(3).

$$(+)\ O_2 + 2H_2O + 4e^- \rightarrow 4OH^- \quad \Phi^\circ = 0.40\ V \tag{1}$$

$$(-)\ 2Mg + 4OH^- \rightarrow 2Mg(OH)_2 + 4e^- \quad \Phi^\circ = -2.69\ V \tag{2}$$

$$\text{Overall}\ 2Mg + O_2 + 2H_2O \rightarrow 2Mg(OH)_2 \quad E^\circ = 3.09\ V \tag{3}$$

The major problem in using Mg/air batteries is the low Coulombic efficiency of the traditional Mg plate electrode and the high level of polarization during the discharge process. The electrolyte for Mg/air batteries, which is a critical factor that influences their electrochemical performance, must also satisfy the objectives of low anodic polarization, a uniform corrosion rate of Mg, and fast sedimentation of the final anodic product ($Mg(OH)_2$) in the electrolyte.

Figure 3 I displays the linear sweep voltammograms (current density (J) versus potential (Φ)) of Mg electrodes made from commercial Mg powder in three different electrolytes: $Mg(ClO_4)_2$ (1.6 M) (a), a mixed solution containing $Mg(NO_3)_2$ (2.6 M) and $NaNO_2$ (3.6 M) (b), and 14 wt% NaCl (c). The anodic dissolution current densities of the Mg electrodes in the three electrolytes all increase as the potential sweeps from −1.5 to −0.5 V. As for electrolyte c, the anodic dissolution current density increases quickly at

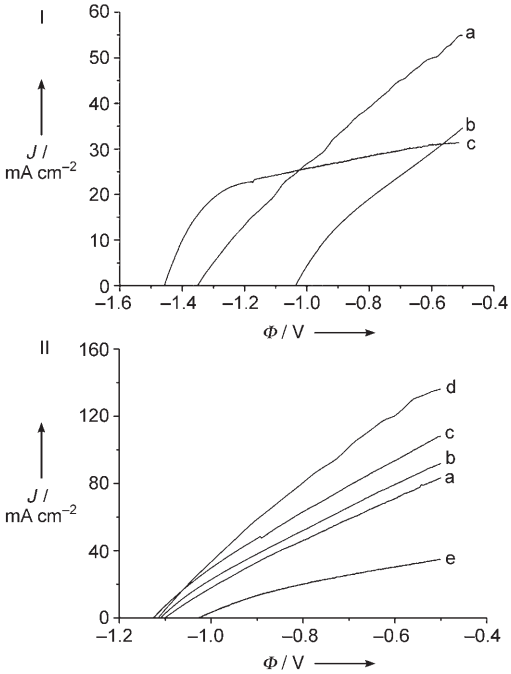

Figure 3. I) Linear sweep voltammograms of Mg electrodes made from commercial Mg powder in three different electrolytes: $Mg(ClO_4)_2$ (1.6 M) (a), a mixed solution of $Mg(NO_3)_2$ (2.6 M) and $NaNO_2$ (3.6 M) (b), and 14 wt% NaCl (c); II) linear sweep voltammograms of different Mg electrodes made from the various as-prepared Mg structures: sample A (a), sample B (b), sample C (c), sample D (d), and commercial Mg powder (e) with a mixed electrolyte solution of $Mg(NO_3)_2$ (2.6 M) and $NaNO_2$ (3.6 M). Scan rate: 20 $mV s^{-1}$; potential range: −1.50 to −0.50 V versus Ag/AgCl saturated with KCl.

first in the potential range −1.45 to −1.25 V and then slows down when the potential sweeps to more positive values; this behavior is due to the formation of a passive film of $Mg(OH)_2$ on the Mg electrode surface. In electrolytes a and b, however, no obvious passivation phenomena are observed. Moreover, the starting potentials of the Mg anodic dissolution in the three electrolytes are quite different (−1.35, −1.03, and −1.45 V for electrolytes a, b, and c, respectively). Although a more negative anodic dissolution potential indicates a higher open circuit voltage for the Mg/air battery, the corrosion problem of Mg electrodes, which reduces the shelf life and operating life of the battery, is much more acute in electrolytes a and c. The overall reaction for the corrosion of a Mg electrode can be expressed by Equation (4).

$$Mg + 2\,H_2O \rightarrow Mg(OH)_2 + H_2\uparrow \quad (4)$$

With regard to electrolytes a and c, a large number of bubbles can be seen around the Mg electrode during our experiment, thus indicating the rapid release of H_2 gas and serious self-discharge problems; few bubbles were observed in electrolyte b. It has been demonstrated in detail by Sathyanarayana and co-workers[17] that a mixed electrolyte containing $Mg(NO_3)_2$ and $NaNO_2$ is better than a variety of other electrolytes (especially conventional halide or perchlorate electrolytes) in terms of low corrosion rate on open circuit, which can keep the Mg anode in an activated state for about a year, high Faradaic efficiency for Mg anodic dissolution (higher than 90% at a current density of above 20 mA cm^{-2}), and uniform pattern of corrosion. Consequently, an electrolyte of $Mg(NO_3)_2$ and $NaNO_2$ solution should be suitable for a Mg/air battery containing Mg anodes with a high surface area, especially those made from Mg nanomaterials. Moreover, Mg/air batteries are generally operated either as "reserve" batteries, in which the electrolyte solution is added to the cell only when required to begin the discharge, or as "mechanically rechargeable" batteries, which have replacement anode units available. With respect to our laboratory-made Mg/air batteries, the controllable air vent is closed during battery storage and the anode is isolated from the electrolyte fluid prior to the first or successive uses of the cell. Therefore, the self-discharge problem can be readily controlled and inhibited to some extent.

Figure 3 II shows the linear sweep voltammograms of different Mg electrodes made from various as-synthesized Mg nano/mesostructures and commercial Mg powder in an electrolyte of $Mg(NO_3)_2$ (2.6 M) and $NaNO_2$ (3.6 M). The starting potentials of the Mg anodic dissolution for the electrodes made from Mg nano/mesostructures are shifted to more negative potentials of approximately −1.10 to −1.13 V compared with the value of −1.03 V for the commercial Mg powder electrode. Furthermore, the anodic dissolution current densities of the electrodes made from the Mg nano/mesostructures are much higher than that of the electrode made from the Mg powder; the sequence of current densities from highest to lowest is d > c > b > a > e. These results indicate that the electrochemical activity of vapor-deposited Mg structures is significantly higher than that of commercial Mg powder.

Figure 4 shows representative discharge curves (cell potential (E) versus discharge time (t)) for Mg/air batteries made from samples A and D, at a constant current of 0.5 mA

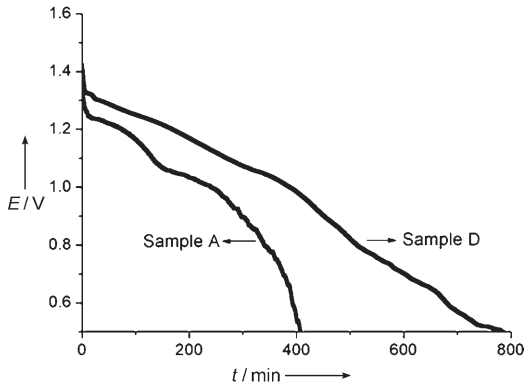

Figure 4. Representative discharge curves of the Mg/air batteries made from samples A and D, at a constant current of 0.5 mA and a temperature of 25 °C.

and a temperature of 25 °C in the voltage range 1.5–0.5 V. The open-circuit voltage of the battery made from sample D is approximately 1.42 V and is higher than that of the battery made from sample A (approximately 1.36 V). In addition, the battery made from sample D also exhibits a higher discharge voltage and a much longer discharge time than the battery made from sample A, thus indicating its higher energy density. The discharge curves of the batteries made from samples B and C show similar voltage profiles to those of samples A and D; the discharge times of samples B and C are approximately 480 and 620 min, respectively.

Table 1 summarizes the energy densities of the Mg/air batteries made from the as-synthesized Mg structures at different discharge current densities. The energy densities of all the batteries decrease with increasing discharge current density. The Mg/air battery made from sample D shows the highest energy density among the four batteries. At a current density of 50 mA cm^{-2}, the energy density of the Mg/air battery made from sample D is still 305 W h kg^{-1}, approximately 54.0% of its energy density at 5 mA cm^{-2}, while those of the Mg/air batteries made from samples A–C are approximately 24.6, 30.3, and 43.9% of their energy densities at 5 mA cm^{-2}, respectively. It is therefore apparent that the sequence of high-rate discharge ability from best to worst is D > C > B > A.

According to the results presented above, the Mg/air batteries made from vapor-deposited Mg nano/mesostruc-

Table 1: Energy densities of the Mg/air batteries made from the various as-prepared Mg structures, at different discharge current densities.

Mg structure	Energy density [W h kg^{-1}] at discharge current densities [mA cm^{-2}] of			
	5	10	25	50
Sample A	285	230	153	70
Sample B	346	282	197	105
Sample C	455	385	283	200
Sample D	565	494	402	305

tures, especially the battery made from the Mg sea-urchin-like nanostructures, display much better electrochemical properties (high gravimetric energy density) than the various existing power sources (see Supporting Information). It is generally believed that chemical and physical properties can be altered considerably when downsizing materials into the nanoscale region. With decreasing particle size, an increasing proportion of the total number of the atoms lie near or at the surface, thus making the materials more active for the electrochemical reaction and significantly enhancing the utilization efficiency of the Mg electrode. Furthermore, the battery made from the Mg sea-urchin-like nanostructures exhibits the best high-rate discharge capability, which is critical for high-power-output battery systems. This may be attributable to the porous and network structure of these nanostructures, which contributes to the low anodic polarization/corrosion of Mg and fast sedimentation of the anodic product ($Mg(OH)_2$) in the electrolyte. The polarization of the Mg electrode increases with increasing discharge current density. The high specific surface areas of the Mg sea-urchin-like nanostructures can help to reduce the real current density for the electrode during the discharge process and lead to a relatively low level of polarization for the Mg electrode, which is favorable for improving the energy density and high-rate discharge capability of the battery.

Experimental Section

The experimental setup consisted of a conventional tube furnace (68.0 cm in length, 40.0 cm in diameter), a horizontal stainless-steel tube (80.0 cm in length, 1.6 cm in diameter), and a gas-flow control system (see Supporting Information). In a typical preparation, Mg powder (99.8% purity, Alfa Aesar) was put into a W boat at the center of the stainless-steel tube. The tube furnace was heated at a rate of 30 °C min^{-1} to a temperature of 850 or 950 °C and maintained at this temperature for 1 h, under a constant flow of high-purity Ar (>99.995%). The flow rates of Ar were controlled at 400 or 800 cm^3 min^{-1} during the heating process. Silver-gray wool-like products were obtained on the surface of the substrate in the cooler region of the stainless-steel tube at a deposition temperature of approximately 300 °C. After the chamber had cooled naturally to ambient temperature, the products were collected and kept in a vacuum desiccator for further analysis.

The as-prepared samples were characterized by powder XRD (Rigaku D/max-2500 X-ray generator, $Cu_{K\alpha}$ radiation), SEM (Philips XL-30 and JEOL JSM-6700F field emission), TEM and HRTEM (FEI Tecnai 20, 200 kV), and BET nitrogen adsorption/desorption measurements (Shimadzu-Micromeritics ASAP 2010 Instrument).[18]

Magnesium electrodes were prepared in a glove box filled with Ar (99.995%) by filling a glass tube (2.1 mm in diameter) containing a Cu wire as collector with a mixture of 65 wt% active materials (vapor-deposited Mg products or commercial Mg powder), 25 wt% acetylene black, and 10 wt% poly(tetrafluoroethylene) (PTFE) solution. The electrochemical properties of these electrodes were investigated with a Parstat 2273 potentiostat/galvanostat analyzer (AMTECT Company) in an electrochemical cell that contained the Mg working electrode, a Pt counter electrode, and a Ag/AgCl-KCl (saturated) reference electrode.

The laboratory-made Mg/air batteries were assembled with a Mg anode and an air cathode. The Mg anode was prepared in a glove box filled with Ar (99.995%) in the presence of an O_2 scavenger and an Na drying agent. The air electrodes were composed of two layers: an $La_{0.6}Ca_{0.4}CoO_3$ perovskite catalyst layer on the electrolyte side and a hydrophobic gas-diffusion layer on the gas side.[19] The electrolyte was a mixed solution containing $Mg(NO_3)_2$ (2.6 M) and $NaNO_2$ (3.6 M). The batteries were tested with an Arbin charge–discharge device.

Received: January 10, 2006
Revised: June 11, 2006
Published online: August 4, 2006

Keywords: batteries · electrochemistry · magnesium · materials science · nanostructures

[1] a) C. Burda, X. B. Chen, R. Narayanan, M. A. El-Sayed, *Chem. Rev.* **2005**, *105*, 1025; b) C. T. Campbell, *Science* **2004**, *306*, 234.
[2] a) F. Raimondi, G. G. Scherer, R. Kotz, A. Wokaun, *Angew. Chem.* **2005**, *117*, 2228; *Angew. Chem. Int. Ed.* **2005**, *44*, 2190; b) H. P. Liang, H. M. Zhang, J. S. Hu, Y. G. Guo, L. J. Wan, C. L. Bai, *Angew. Chem.* **2004**, *116*, 1566; *Angew. Chem. Int. Ed.* **2004**, *43*, 1540.
[3] Y. N. Xia, P. D. Yang, Y. G. Sun, Y. Y. Wu, B. Mayers, B. Gates, Y. D. Yin, F. Kim, H. Q. Yan, *Adv. Mater.* **2003**, *15*, 353.
[4] a) X. G. Wen, Y. P. Fang, S. H. Yang, *Angew. Chem.* **2005**, *117*, 3628; *Angew. Chem. Int. Ed.* **2005**, *44*, 3562; b) S. R. C. Vivekchand, G. Gundiah, A. Govindaraj, C. N. R. Rao, *Adv. Mater.* **2004**, *16*, 1842.
[5] a) R. W. P. Wagemans, J. H. van Lenthe, P. E. de Jongh, A. J. van Dillen, K. P. de Jong, *J. Am. Chem. Soc.* **2005**, *127*, 16675; b) H. Imamura, T. Nobunaga, M. Kawahigashi, S. Tsuchiya, *Inorg. Chem.* **1984**, *23*, 2509.
[6] a) P. Dai, P. H. Dussault, T. K. Trullinger, *J. Org. Chem.* **2004**, *69*, 2851; b) B. Bogdanović, *Angew. Chem.* **1985**, *97*, 253; *Angew. Chem. Int. Ed. Engl.* **1985**, *24*, 262.
[7] J. A. Cowan, *The Biological Chemistry of Magnesium*, VCH Publishers, New York, **1995**.
[8] a) D. Aurbach, Z. Lu, A. Schechter, Y. Gofer, H. Gizbar, R. Turgeman, Y. Cohen, M. Moshkovich, E. Levi, *Nature* **2000**, *407*, 724; b) A. Brenner, *J. Electrochem. Soc.* **1996**, *143*, 3133.
[9] Y. K. Zhang, S. J. Liao, Y. H. Fan, *J. Nanopart. Res.* **2001**, *3*, 23.
[10] a) L. Lu, M. O. Lai, W. Liang, *Compos. Sci. Technol.* **2004**, *64*, 2009; b) J. L. Bobet, E. Grigorova, M. Khrussanova, M. Khristov, P. Stefanov, P. Peshev, D. Radev, *J. Alloys Compd.* **2004**, *366*, 298.
[11] H. Li, F. Pederiva, G. H. Wang, B. L. Wang, *J. Appl. Phys.* **2004**, *96*, 2214.
[12] a) M. Winter, R. J. Brodd, *Chem. Rev.* **2004**, *104*, 4245; b) J. M. Tarascon, M. Armand, *Nature* **2001**, *414*, 359.
[13] D. Linden, T. B. Reddy, *Handbook of Batteries*, 3rd ed., McGraw-Hill, New York **2002**.
[14] a) A. Weidenkaff, S. G. Ebbinghaus, T. Lippert, *Chem. Mater.* **2002**, *14*, 1797; b) S. Muller, K. Striebel, O. Haas, *Electrochim. Acta* **1994**, *39*, 1661.
[15] Y. D. Yin, G. T. Zhang, Y. N. Xia, *Adv. Funct. Mater.* **2002**, *12*, 293.
[16] a) X. Zhang, S. H. Yang, H. Knickel, *J. Power Sources* **2004**, *128*, 331; b) X. Y. Wang, P. J. Sebastian, M. A. Smit, H. P. Yang, S. A. Gamboa, *J. Power Sources* **2003**, *124*, 278; c) E. Deiss, F. Holzer, O. Haas, *Electrochim Acta* **2000**, *47*, 3995.
[17] a) S. Sathyanarayana, N. Munichandraiah, *J. Appl. Electrochem.* **1981**, *11*, 33; b) R. P. Hamlen, E. C. Jerabek, J. C. Ruzzo, E. G. Siwek, *J. Electrochem. Soc.* **1969**, *116*, 1588.
[18] a) F. Y. Cheng, J. Chen, X. L. Gou, P. W. Shen, *Adv. Mater.* **2005**, *17*, 2753; b) J. Chen, L. N. Xu, W. Y. Li, X. L. Gou, *Adv. Mater.* **2005**, *17*, 582; c) X. Wang, J. Zhuang, J. Chen, K. B. Zhou, Y. D. Li, *Angew. Chem.* **2004**, *116*, 2051; *Angew. Chem. Int. Ed.* **2004**, *43*, 2017.
[19] D. Chartouni, N. Kuriyama, T. Kiyobayashi, J. Chen, *Int. J. Hydrogen Energy* **2002**, *27*, 945.

